(Received 10 April 2025, Accepted 3 August 2025, Scheduled 13 August 2025)

A Novel Broadband Cross-Loop Dipole Antenna with Coupling Slots

Yanzheng Chen*

Southwest China Institute of Electronic Technology, China

ABSTRACT: A novel broadband $\pm 45^\circ$ dual-polarization antenna is presented. By introducing coupling slots on the loop dipole arms of the antenna, multi-resonance performance occurs so that the impedance bandwidth is greatly widened. An enhanced impedance bandwidth about 92.5% with VSWR < 2 is obtained at two ports, corresponding to the frequency region of 1.61–4.38 GHz. In the frequency range of 1.61–3.8 GHz, a gain of 8.2 ± 2.2 dBi is obtained. For the frequencies beyond 3.8 GHz, the gain drops sharply and goes down to 1.1 dBi at 4 GHz. Within the operating frequencies, a port-to-port isolation > 22.5 dB is achieved. Especially, the proposed antenna has a very simple configuration and is easy to be fabricated. A mechanical prototype of the antenna has been manufactured and measured. The measurement results have good agreement with the simulations. The work principle and detailed descriptions of the antenna are presented in the paper.

1. INTRODUCTION

In the last decade, many broadband complementary dipole antennas have been intensively studied and applied in mobile communication systems [1–17]. These dipole antennas can be divided into three general types, including magneto-electric dipole antennas, in-phase binary dipole antennas, and cross-dipole antennas. The three kinds of antennas have similar principles and achieve stable radiation patterns by applying complementary concept. Compared with the traditional printed dipole antennas [18, 19], complementary dipole antennas have a more stable radiation pattern, higher gain, and wider impedance bandwidth. Magnetoelectric dipole antenna is first proposed in [1]. Adopting a shorted planar dipole with vertical bending to the ground plane and a Γ-shaped feeding probe, an electric dipole is ingeniously combined with a magnetic dipole so that complementary radiation is achieved [2, 3]. In [4], Chu and Luo present an in-phase binary dipole antenna, which achieves constant radiation pattern and virtually identical E- and H-planes in the wide frequency range. Compared with the first two kinds of complementary dipole antennas, the cross-dipole antenna is more suitable for applications in base stations, since it can be easily designed as a dual-polarized antenna. Through two orthogonally-placed dipoles, the complementarity of the radiation pattern is achieved in the two polarization planes. With the rapid development of mobile base-station communication technology, the researches on the cross-dipole antenna are burgeoning [5–16].

The researchers usually adopt loop dipole [5–7], bow-tie dipole [8–16], octagonal dipole [9] or fan-shaped dipole [11, 15, 17] as cross-dipole antenna's radiation element, under which a plate or box-reflector is placed to ensure the unidirection of radiation. In order to cover more services of mobile communication, engineers attempt to broaden the bandwidth of the cross-dipole antenna. Many methods for expanding bandwidth have been proposed, including parasitic-loading technology [10], multi-dipoles usage [11, 15, 16], and shared-aperture technology [14]. However, these methods have enhanced the structure complexity of the antennas, leading to high manufacturing cost.

In this communication, we propose a novel and simple $\pm 45^\circ$ dual-polarization antenna with a very wide impedance bandwidth. By adding two coupling slots to the arm of cross-loop dipole, a capacitor is introduced so that a parallel resonance occurs in the loop arm of the parasitic dipole. Therefore, the impedance matching and gain of the antenna are greatly improved. In order to demonstrate the distinguished performance of the proposed antenna, a comparison with the related antennas [10–17] is displayed in Table 1. As detailed, in order to broaden the bandwidth, additional dielectric and ground layers have been added in the design of the antennas [10, 11, 14–16]. Thus, the structure complexity and processing costs of the antennas are enhanced. In [13], although the antenna has only one dielectric layer and one grounding plate, an inverted pyramidal cavity is used as a reflector, which increases the difficulty of processing and prohibits the antenna forming an array. Through comprehensive comparisons, it is clear that the proposed antenna has outstanding performance with simple configuration.

2. ANTENNA CONFIGURATION

The presented antenna's configuration, depicted in Fig. 1, is engineered for optimal performance. The detailed structural parameters in Table 2 offer insights into the antenna's geometry and dimensions. Fig. 1(c) reveals the orthogonal arrangement of two crossed dipoles, and a loop structure with two coupling slots is chosen as a dipole element. One portion of the dipoles forms coplanar transmission lines, which are ladder shaped and serve as impedance transformers. Through capacitive coupling, the antenna is excited by two Y-shaped feed-

* Corresponding author: Yanzheng Chen (yzchen@uestc.edu.cn).

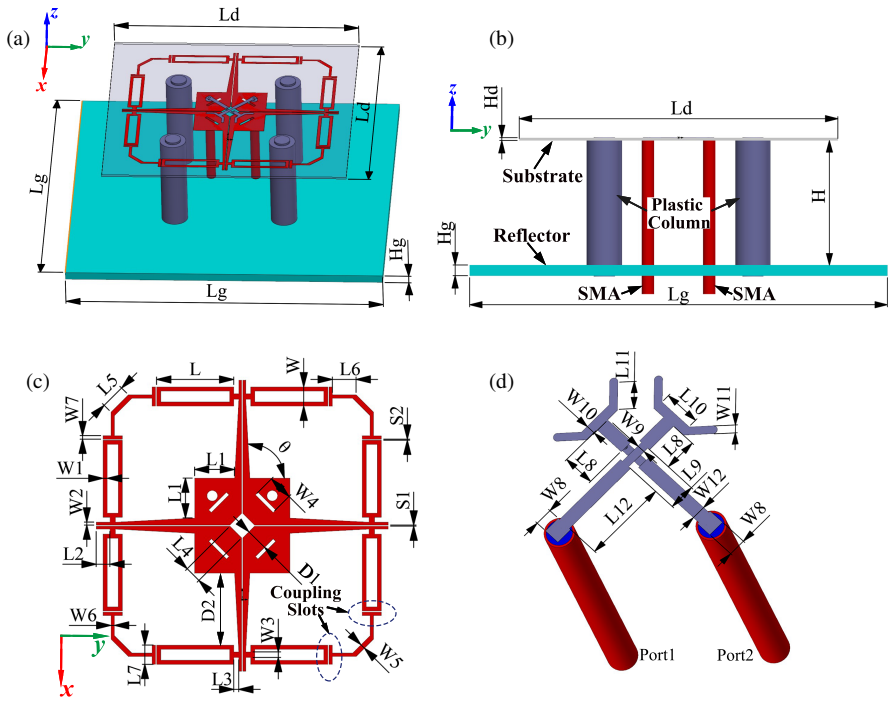

FIGURE 1. Configuration of the proposed antenna. (a) Three-dimensional view; (b) Side view; (c) Dipole elements; (d) Y-shaped feeding lines.

TABLE 1. A comparison between the proposed antenna and the same-type antennas.

Antenna	Overall size (λ_{min})	BW (GHz)	BW (%)	Gain (dBi)	Isolation (dB)	Structure complexity	Number of dielectric and grounding layers
Ref. [10]	$0.78 \times 0.78 \times 0.24$	1.67–2.37 (VSWR $<$ 2) 3.26–3.67 (VSWR $<$ 2)	NG	8.1 ± 0.4 6.6 ± 0.5	$>$ 35	complex	2&1
Ref. [11]	$0.51 \times 0.51 \times 0.23$	0.7–0.96 (RL $>$ 10) 1.7–3 (RL $>$ 10) 3.3–3.8 (RL $>$ 10)	NG	5.5 8 5.5	$>$ 20	complex	2&1
Ref. [12]	$0.82 \times 0.82 \times 0.24$	2.35–2.8 (RL $>$ 10) 3.15–3.7 (RL $>$ 10)	NG	8.4 7.7	$>$ 25	complex	5&1
Ref. [13]	$0.69 \times 0.69 \times 0.19$	1.6–3.83 (RL $>$ 10)	82.1%	8.3 ± 2.1	$>$ 43	simple	1&1
Ref. [14]	$0.75 \times 0.75 \times 0.19$	1.60–2.70 (RL $>$ 10) 3.28–3.80 (RL $>$ 10) 4.75–5.18 (RL $>$ 10)	NG	7.6 8.6 9.5	$>$ 20	complex	3&1
Ref. [15]	$0.6 \times 0.6 \times 0.22$	1.7–3.22 (VSWR $<$ 2)	61.8%	$\sim$5.7	$>$ 29	complex	1&2
Ref. [16]	$0.85 \times 0.85 \times 0.14$	3.3–3.6 (RL $>$ 10) 4.8–5 (RL $>$ 10)	NG	$\sim$7 $\sim$8.2	$>$ 25	complex	3&1
Ref. [17]	$0.67 \times 0.67 \times 0.34$	1.68–2.90 (RL $>$ 10)	53.3%	6.6 ± 2.2	$>$ 34.5	complex	NG
This work	$0.65 \times 0.65 \times 0.19$	1.61–4.38 (VSWR $<$ 2)	92.5%	8.2 ± 2.2 (1.61–3.8 GHz)	$>$ 22.5	simple	1&1

λ_{min} is the free-space wavelength referring to the lowest operational frequency.

ing lines with notches. To further boost impedance matching, strategically positioned slots are incorporated into the dipole elements, both in front of and behind the Y-shaped feeding lines. The crossed dipoles are meticulously fabricated on the lower side of a Rogers 5880 substrate, characterized by a permittivity of 2.2 and a loss tangent of 0.0009. Simultaneously, the Y-shaped feeding lines are carefully plated to the upper side of the substrate. To prevent unwanted overlap, a segment of one Y-shaped feeding line is positioned on the substrate's lower side and connected to the upper section through a shorting pin. In the pursuit of achieving unidirectional radiation, a square reflector is strategically placed beneath the radiators. The connection between the substrate and reflector is facilitated by four plastic columns with a permittivity of 2.1 and a radius of 5 mm. This

TABLE 2. Structural parameters of the proposed antenna.

Parameters	Lg	Hg	Ld	Hd	H	L	W	$L1$
Value/mm	122	1	94	0.79	35	22	5.5	11.39
Parameters	$W1$	$L2$	$W2$	$L3$	$W3$	$L4$	$W4$	$L5$
Value/mm	1.2	3.9	0.85	1.4	2	4.7	7.1	7
Parameters	$W5$	$L6$	$W6$	$L7$	$W7$	$L8$	$W8$	$L9$
Value/mm	1.43	6.8	1	5.5	1	3.76	1	3
Parameters	$W9$	$L10$	$W10$	$L11$	$W11$	$L12$	$W12$	$D1$
Value/mm	1	4.37	1.15	3.2	0.94	9.6	1.6	6.33
Parameters	$D2$	$S1$	$S2$	Parameters		θ		
Value/mm	20.57	0.3	0.3	Value/degree		93.03		

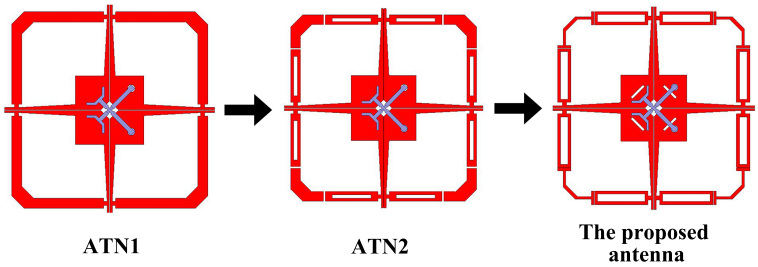

FIGURE 2. Evolution of the presented antenna.

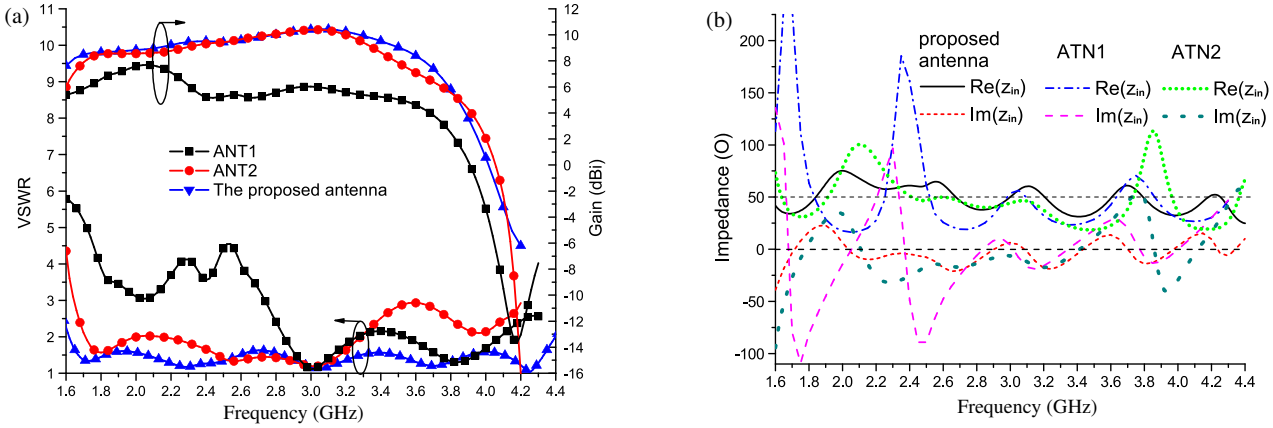

FIGURE 3. Comparison among the ATN 1, ANT 2, and proposed antenna on the VSWR, gain, and input impedance.

meticulous design ensures the antenna's robust performance and efficient radiation characteristics across a broad frequency spectrum.

3. ANALYSIS OF ANTENNA PRINCIPLE

3.1. Circuit Model for the Proposed Antenna

The proposed dipole element is evolved from a cross-loop dipole, as depicted in Fig. 2. The original antenna (ANT 1) is a crossed loop-dipole antenna. ANT 2 is obtained by introducing two coupling slots on the arms of ANT 1. Based on ANT 2, we add two slots on dipoles element in front of and behind the Y-shaped feeding lines and optimize the structure to improve further impedance matching. Voltage standing wave ratio (VSWR), gain, and input impedance comparisons among the three kinds of antennas are displayed in Fig. 3. It can be observed that the VSWR and gain of the cross-dipole antenna are greatly improved by introducing coupling slots on the loop dipole. In the low-frequency range, the input impedance of ANT 1 has a significant fluctuation, leading to a poor impedance matching. By adding the coupling slots (ANT 2), the variation of the input impedance tends to flatten out, as shown in Fig. 3(b). For describing the effects of the coupling slots theoretically, we present a simple equivalent schematic of the proposed antenna [20], as shown in Fig. 4.

For simplicity, the effects of the Y-shaped feed lines are ignored here. By adding coupling slots, the arms of the loop dipole are divided into two parts, which are denoted as

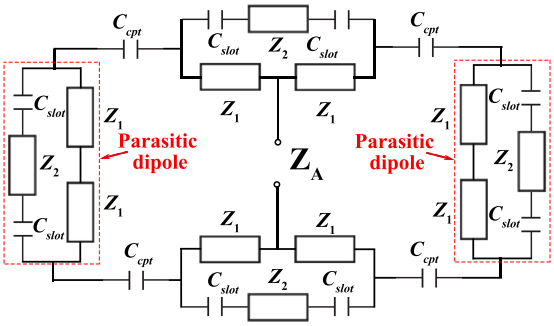

FIGURE 4. Equivalent circuit model of the presented antenna.

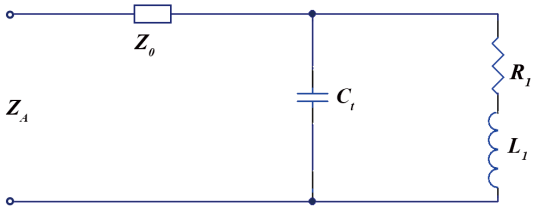

FIGURE 5. Simplified circuit model of the presented antenna.

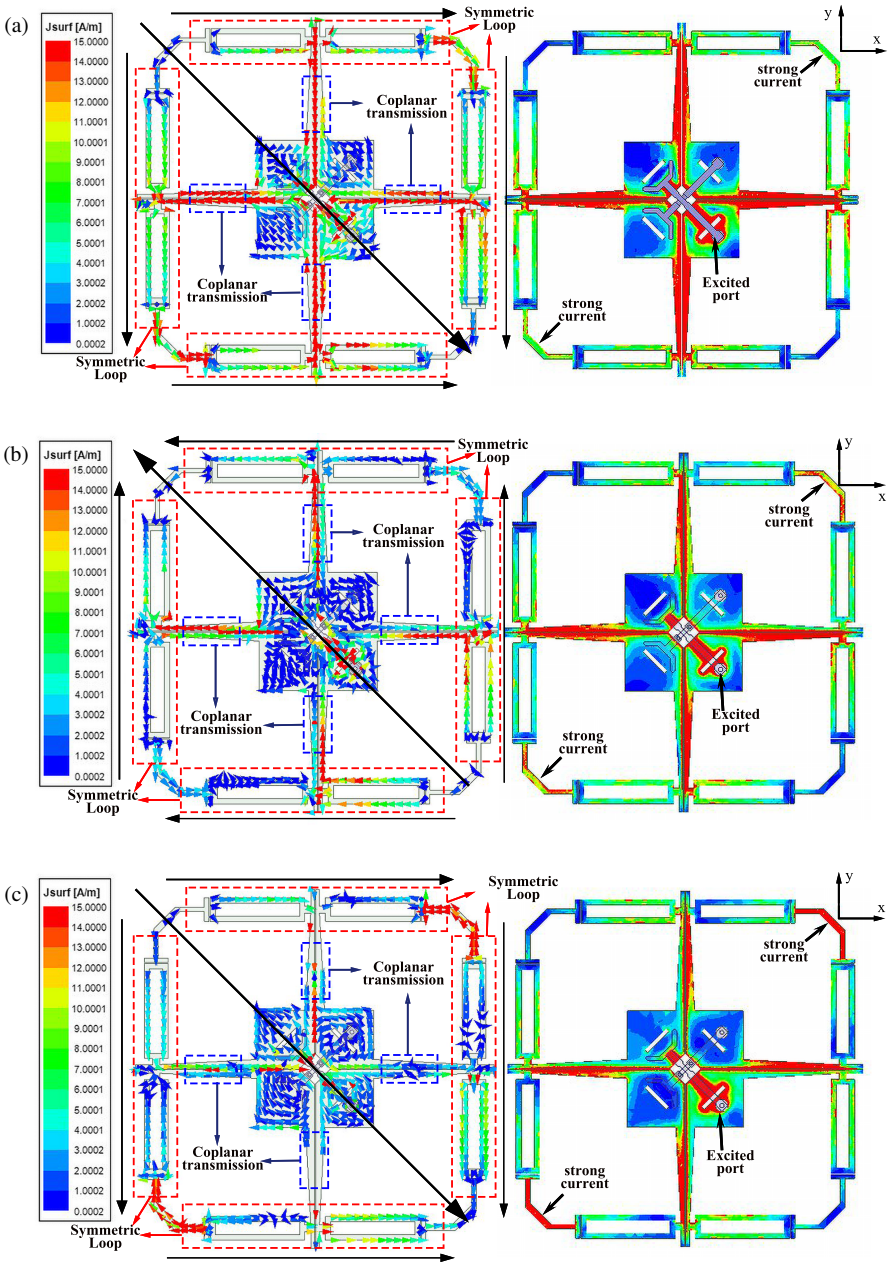

FIGURE 6. Current distributions on the crossed dipoles (vector value and complex magnitude when only one port is stimulated). (a) 1.7 GHz; (b) 2.7 GHz; (c) 3.7 GHz.

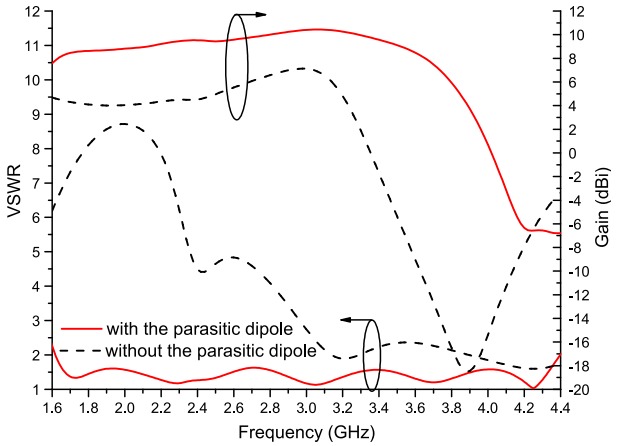

FIGURE 7. VSWRs and gains with and without the parasitic dipole.

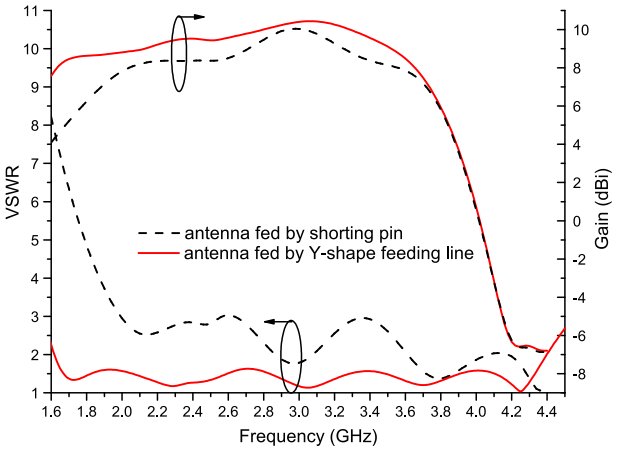

FIGURE 8. Comparison between the antenna fed by shorting pins and that by Y-shape feeding lines.

impedances $2Z_1$ and Z_2, respectively. Z_A is used to represent the input impedance of the antenna. The coupling slots is represented as a capacitance C_{slot}, and the gap between the two coplanar striplines is treated as a capacitor C_{cpt}.

Based on Fig. 4 and methods of circuit analysis, we can get

$$Z_A = Z_1 + \frac{z_1\left(z_2 + \frac{2}{jwC_{slot}}\right)}{2z_1 + z_2 + \frac{2}{jwC_{slot}}} + \frac{1}{jwC_{cpt}}. \quad (1)$$

where w is the angular frequency. It can be seen that only the second term on the right side of Eq. (1) contains C_{slot}, and the term represents the impedance of the parasitic dipole branch. Thus, the coupling slots mainly affect the parasitic dipole branch. By adjusting the position and size of the coupling slots, parallel resonance can occur in the parasitic dipole branches, and the bandwidth of the antenna can be widened.

Based on Eq. (1), we can simplify the equivalent schematic in Fig. 4. Suppose $z_1 = R_1 + jwL_1$, $z_2 = R_2 + jwL_2$, and $z_0 = z_1 + 1/jwC_{cpt}$. Because z_1 and C_{cpt} form a coplanar stripline which has stable impedance, we set it as $z_0 = z_1 + 1/jwC_{cpt}$. Owing to $R_2 \approx 0$ (z_2 represents a short stub), it can be ignored. Assuming that the branch of z_2 is capacitive after introducing the coupling slots, we can get $z_2/2+1/(jwC_{slot}) = 1/jwC_t$ and $C_t = C_{slot}/2(1 - w^2L_2C_{slot})$. Fig. 5 shows the simplified circuit model [3]. Based on it, we can obtain the resonant angular frequency w_0 and resonant impedance R_0, as shown in Eq. (2).

$$w_0 = \sqrt{\frac{1}{L_1C_t} - \frac{R_1^2}{L_1^2}}, \quad R_0 = \frac{L_1}{R_1C_t}. \quad (2)$$

It can be seen that the circuit can resonate at the desired frequency by adjusting the value of C_t. The resonant impedance is related to C_t, and a bigger C_t leads to a decrease of the resonant impedance R_0. Therefore, after introducing the coupling slots, the real part of the input impedance at low resonant frequency has decreased, as shown in Fig. 3(b).

3.2. Current Distribution of the Presented Antenna

The current distributions on the crossed dipoles at 1.7 GHz, 2.7 GHz, and 3.7 GHz are depicted in Fig. 6, with the directions of the total current indicated by thick black arrows. It is observable that there is a notable concentration of current on the arms of the parasitic dipole, and the current forms a loop. That is, parallel resonance occurs on the parasitic dipole, which can be regarded as a magnetic dipole. The direction of the total current on the dipoles are in the direction of $-45°$ or $-225°$ at all frequencies. The summed current is primarily determined by the current distributions on the symmetrical loop. The currents on the coplanar transmission lines nullify each other owing to their symmetric arrangement. Simultaneously, each coplanar transmission line involves two microstrip lines, on which the currents have opposite directions and can be offset in whole or in part. In general, the coplanar transmission lines are non-radioactive and have little impact on the antenna's radiation performance. The dipole can be seen as a half-wave or full-wave dipole at low frequencies. As the frequency increases, the length of the dipole extends beyond a wavelength, resulting in the occurrence of reverse current on the dipole. Initially, the reverse current primarily spreads along the coplanar transmission lines, and the current's direction on each symmetrical loop remains uniform. Consequently, the antenna can sustain high gain within a specific frequency band when operating in higher-order modes. However, once the frequency surpasses a specific threshold, such as 4 GHz, reverse current arises on the symmetrical loop, adversely affecting the radiation performance of the crossed dipoles.

4. PARAMETRIC STUDY

The antenna undergoes simulation and optimization using full-wave simulation software, providing crucial guidance for the mechanical manufacturing process. A parametric analysis is conducted to clarify how the antenna's parameters influence its performance. To simplify the analysis, only one port is activated at a time, while the other parameters are kept constant during the examination of each individual parameter.

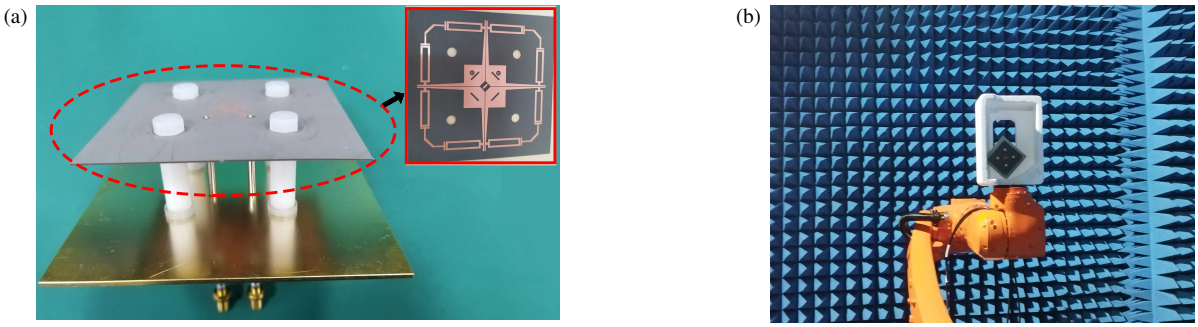

FIGURE 9. Antenna prototype. (a) Photograph of the proposed antenna; (b) Measurement scenario.

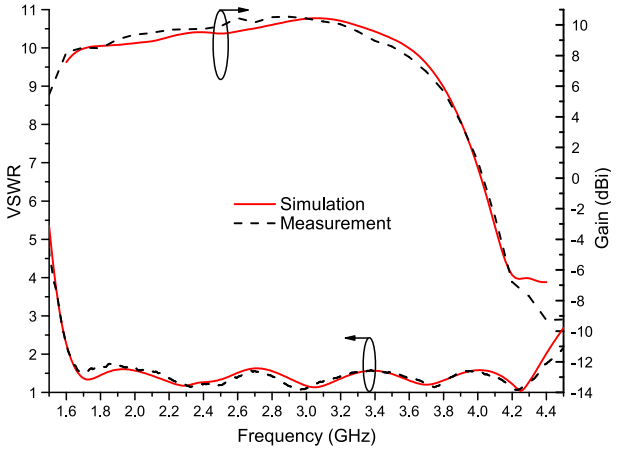

FIGURE 10. Simulated and measured VSWRs and gains of port 1.

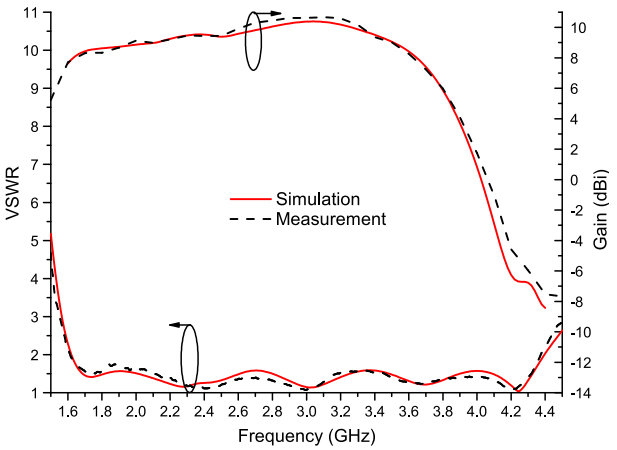

FIGURE 11. Simulated and measured VSWRs and gains of port 2.

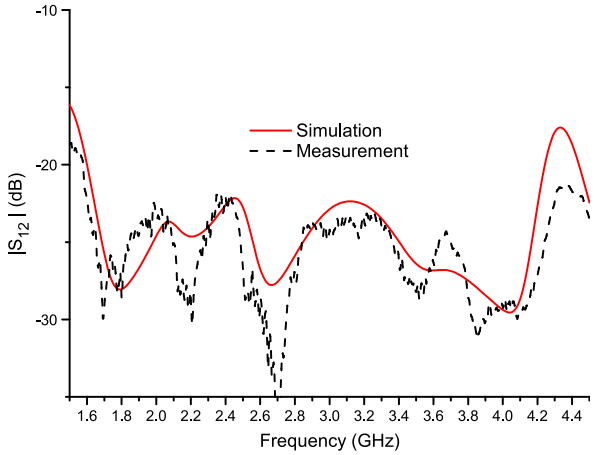

FIGURE 12. Simulated and measured port-to-port isolations of the antenna.

4.1. Effects of the Parasitic Dipole

Being different from the traditional crossed loop-dipole antenna [5–7], one kind of loop dipole with coupling slots is adopted in the proposed antenna. While one dipole is actively stimulated, the other is considered as a parasitic element. A parametric investigation into the parasitic dipole is conducted to comprehend its effects. Fig. 7 illustrates the VSWRs and gains with and without the parasitic dipole. It is evident that the parasitic dipole significantly influences the antenna's performance across the entire frequency range. Removal of the parasitic dipole results in the disappearance of some resonant frequencies and a deterioration in impedance matching, particularly in the low-frequency region. Simultaneously, the parasitic dipole markedly enhances the antenna's gain, particularly in the high-frequency range. In principle, the introduction of the parasitic dipole causes a segment of the dipole element to form a coplanar transmission line. This not only improves the antenna's impedance matching but also serves as a non-radiative element, suppressing reverse currents on the dipoles at higher-order modes.

4.2. Effects of the Y-Shaped Feeding Line

Two Y-shaped feeding lines activate the presented antenna through capacitive coupling, providing the advantage of expanding the antenna's bandwidth. To confirm the significance of the Y-shaped feeding lines in the design, a parametric analysis is conducted. In Fig. 8, a comparison is made between the antenna fed by shorting pins and the one fed by Y-shaped feeding lines on VSWR and gain. The Y-shaped feeding lines notably enhance the antenna's impedance matching compared to the feeding method of shorting pins. The improvement is credited to the introduction of a capacitor induced by the Y-shaped feeding lines, effectively neutralizing the inductive impedance of the dipole element, especially at lower frequencies.

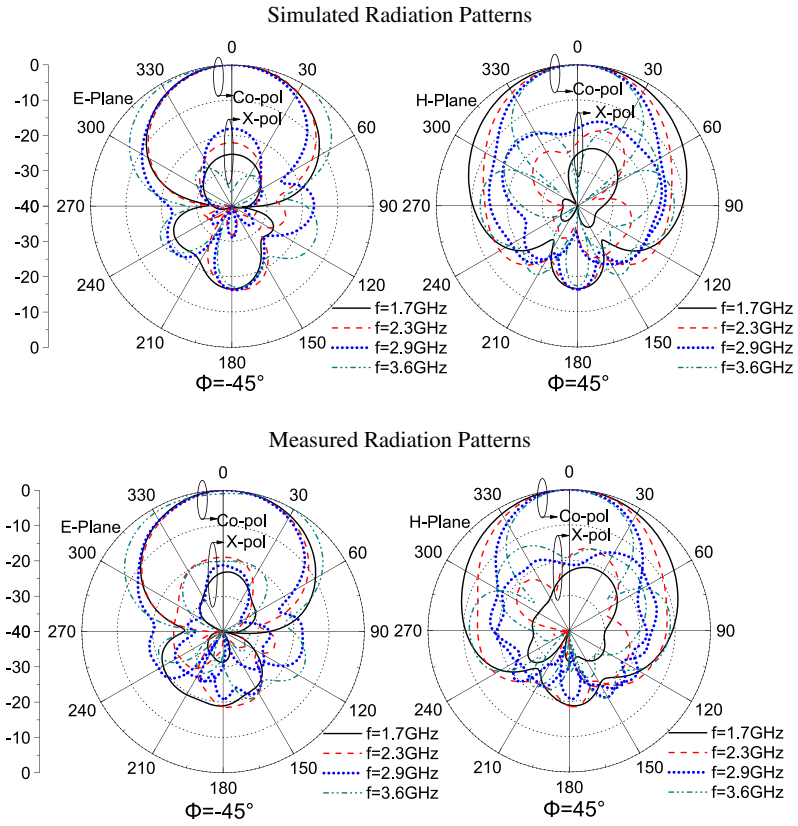

FIGURE 13. Simulated and measured patterns of radiation at port 1.

TABLE 3. The proposed antenna's half-power beamwidth.

Frequency (GHz)	Half-power beam-width (degree)							
	Simulation				Measurement			
	Port 1		Port 2		Port 1		Port 2	
	E-Plane	H-Plane	E-Plane	H-Plane	E-Plane	H-Plane	E-Plane	H-Plane
1.7	60.3	82.8	60.3	82.7	62	81	61	83
2	57.5	73.7	57.5	73.8	58	77	58	71
2.3	58.6	61.1	58.8	61.1	57	62	59	60
2.6	54.7	53.7	54.8	53.6	55	53	55	53
2.9	54.7	51.4	55.0	51.4	56	51	56	52
3.2	56.3	51.4	56.8	51.2	61	54	60	51
3.6	90.3	46.8	90.5	46.9	90	48	91	47

5. MEASUREMENT RESULTS AND DISCUSSION

To validate the design's viability, the antenna is constructed and evaluated using the simulation results. Fig. 9 shows the antenna prototype, whose VSWRs and port-to-port isolation are assessed through a two-port vertical network analyzer, and gains are measured using a microwave anechoic chamber system.

Figures 10 and 11 present the comparisons of the VSWRs and gains between measurements and simulations, respectively. It is clear that the measured results coincide well with the simulations. The prototype's measurement results demonstrate that the proposed antenna's impedance bandwidths cover the frequency range of 1.61–4.38 GHz with VSWR < 2. Measured results show that the gain bandwidths are less than the impedance ones, as predicted by the simulations. The measured gains of 8.2 ± 2.2 dBi are obtained at two ports for the frequency band of 1.61–3.8 GHz. When the frequencies are beyond 3.8 GHz, the gains drop sharply. At 4 GHz, the gains decrease to 1.1 dBi.

The simulation and measurement of the port-to-port isolation are contrasted in Fig. 12, which demonstrates their striking resemblance. A port-to-port isolation of more than 22.5 dB

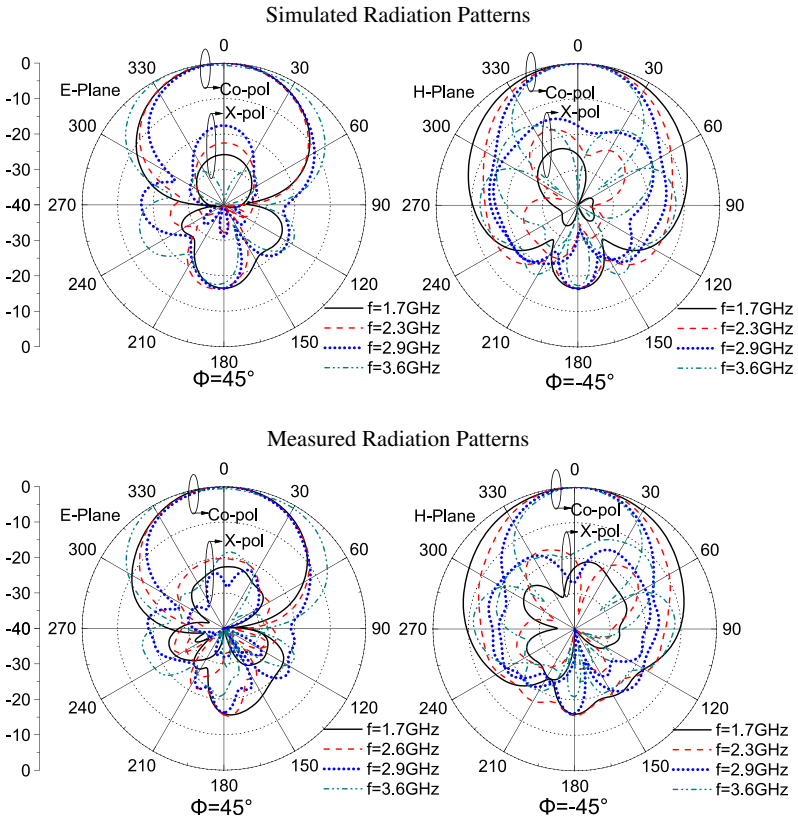

FIGURE 14. Simulated and measured patterns of radiation at port 2.

for the whole operating frequency region has been obtained in the measurement. The far-field patterns of the principle polarisation and cross polarisation at frequencies of 1.7, 2.3, 2.9, and 3.6 GHz, including the simulations and measurements, are presented in Figs. 13 and 14. The measured results fit quite well with simulated ones. In addition, Table 3 lists the half-power beamwidths (HPBWs) from the electromagnetic simulation and experimental measurement. Because the measured HPBWs are from a broad bandwidth, they have large oscillations. For port 1, the measured HPBWs are 72.5 ± 17.5 degrees in E-plane and 64.5 ± 16.5 degrees in H-plane. For port 2, the measurements are 73 ± 18 degrees in E-plane and 65 ± 18 degrees in H-plane.

6. CONCLUSIONS

A novel dual-polarization cross-loop dipole antenna with coupling slots is introduced. The measured outcomes illustrate that the antenna attains an impedance bandwidth exceeding 92.5% for VSWR < 2, within the frequency range of 1.61 to 4.38 GHz across two ports. Across this frequency band, a port-to-port isolation exceeding 22.5 dB is achieved. The gain bandwidths are narrower than the impedance bandwidths. Specifically, within the frequency span of 1.61–3.8 GHz, gains of 8.2 ± 2.2 dBi are realized at both ports. Beyond 3.8 GHz, the gains decline sharply, reaching 1.1 dBi at 4 GHz. The antenna exhibits commendable performance with a remarkably simple structure, suggesting numerous potential applications.

REFERENCES

[1] Luk, K.-M. and H. Wong, "A new wideband unidirectional antenna element," *International Journal of Microwave and Optical Technology*, Vol. 1, No. 1, 35–44, Jun. 2006.

[2] Ge, L. and K. M. Luk, "A low-profile magneto-electric dipole antenna," *IEEE Transactions on Antennas and Propagation*, Vol. 60, No. 4, 1684–1689, Apr. 2012.

[3] Luk, K.-M. and B. Wu, "The magnetoelectric dipole — A wideband antenna for base stations in mobile communications," *Proceedings of the IEEE*, Vol. 100, No. 7, 2297–2307, Jul. 2012.

[4] Chu, Q.-X. and Y. Luo, "A broadband unidirectional multidipole antenna with very stable beamwidth," *IEEE Transactions on Antennas and Propagation*, Vol. 61, No. 5, 2847–2852, May 2013.

[5] Chu, Q.-X., D.-L. Wen, and Y. Luo, "A broadband $\pm 45^\circ$ dual-polarized antenna with Y-shaped feeding lines," *IEEE Transactions on Antennas and Propagation*, Vol. 63, No. 2, 483–490, Feb. 2015.

[6] Mirmozafari, M., G. Zhang, S. Saeedi, and R. J. Doviak, "A dual linear polarization highly isolated crossed dipole antenna for MPAR application," *IEEE Antennas and Wireless Propagation Letters*, Vol. 16, 1879–1882, 2017.

[7] Chen, Y., W. Lin, S. Li, and A. Raza, "A broadband $\pm 45^\circ$ dual-polarized multidipole antenna fed by capacitive coupling," *IEEE Transactions on Antennas and Propagation*, Vol. 66, No. 5, 2644–2649, May 2018.

[8] Li, M., X. Chen, A. Zhang, and A. A. Kishk, "Dual-polarized broadband base station antenna backed with dielectric cavity for 5G communications," *IEEE Antennas and Wireless Propagation Letters*, Vol. 18, No. 10, 2051–2055, Oct. 2019.

[9] Yang, S. J., Y. F. Cao, Y. M. Pan, Y. Wu, H. Hu, and X. Y. Zhang, "Balun-fed dual-polarized broadband filtering antenna without extra filtering structure," *IEEE Antennas and Wireless Propagation Letters*, Vol. 19, No. 4, 656–660, Apr. 2020.

[10] Fu, S., Z. Cao, X. Quan, and C. Xu, "A broadband dual-polarized notched-band antenna for 2/3/4/5G base station," *IEEE Antennas and Wireless Propagation Letters*, Vol. 19, No. 1, 69–73, 2020.

[11] Alieldin, A., Y. Huang, S. J. Boyes, M. Stanley, S. D. Joseph, Q. Hua, and D. Lei, "A triple-band dual-polarized indoor base station antenna for 2G, 3G, 4G and sub-6 GHz 5G applications," *IEEE Access*, Vol. 6, 49 209–49 216, 2018.

[12] Liu, Y., S. Wang, N. Li, J.-B. Wang, and J. Zhao, "A compact dual-band dual-polarized antenna with filtering structures for sub-6 GHz base station applications," *IEEE Antennas and Wireless Propagation Letters*, Vol. 17, No. 10, 1764–1768, Oct. 2018.

[13] Ta, S. X., D. M. Nguyen, K. K. Nguyen, C. D. Ngoc, and N. N. Trong, "Wideband differentially fed dual-polarized antenna for existing and sub-6 GHz 5G communications," *IEEE Antennas and Wireless Propagation Letters*, Vol. 19, No. 12, 2033–2037, Dec. 2020.

[14] Zhou, G.-N., B.-H. Sun, Q.-Y. Liang, S.-T. Wu, Y.-H. Yang, and Y.-M. Cai, "Triband dual-polarized shared-aperture antenna for 2G/3G/4G/5G base station applications," *IEEE Transactions on Antennas and Propagation*, Vol. 69, No. 1, 97–108, Jan. 2021.

[15] Feng, Y., F.-S. Zhang, G.-J. Xie, Y. Guan, and J. Tian, "A broadband and wide-beamwidth dual-polarized orthogonal dipole antenna for 4G/5G communication," *IEEE Antennas and Wireless Propagation Letters*, Vol. 20, No. 7, 1165–1169, Jul. 2021.

[16] Li, M., M. Y. Jamal, C. Zhou, L. Jiang, and L. K. Yeung, "A novel dipole configuration with improved out-of-band rejection and its applications in low-profile dual-band dual-polarized stacked antenna arrays," *IEEE Transactions on Antennas and Propagation*, Vol. 69, No. 6, 3517–3522, Jun. 2021.

[17] Zhao, Z.-B., W.-J. Lu, L. Zhu, and J. Yu, "Wideband wide beamwidth full-wavelength sectorial dipole antenna under dual-mode resonance," *IEEE Transactions on Antennas and Propagation*, Vol. 69, No. 1, 14–24, Jan. 2021.

[18] Ta, S. X., H. Choo, and I. Park, "Broadband printed-dipole antenna and its arrays for 5G applications," *IEEE Antennas and Wireless Propagation Letters*, Vol. 16, 2183–2186, 2017.

[19] Farzami, F., S. Khaledian, B. Smida, and D. Erricolo, "Pattern-reconfigurable printed dipole antenna using loaded parasitic elements," *IEEE Antennas and Wireless Propagation Letters*, Vol. 16, 1151–1154, 2016.

[20] Wen, D.-L., D.-Z. Zheng, and Q.-X. Chu, "A dual-polarized planar antenna using four folded dipoles and its array for base stations," *IEEE Transactions on Antennas and Propagation*, Vol. 64, No. 12, 5536–5542, Dec. 2016.